X-621-70-478
PREPRINT

TMX 65443

SEMIANNUAL VARIATIONS IN THE NEUTRAL COMPOSITION

H.G. MAYR
H. VOLLAND

NOVEMBER 1970

GSFC
GODDARD SPACE FLIGHT CENTER
GREENBELT, MARYLAND

X-621-70-478
PREPRINT

SEMIANNUAL VARIATIONS IN THE NEUTRAL COMPOSITION

H. G. Mayr

H. Volland

November 1970

GODDARD SPACE FLIGHT CENTER

Greenbelt, Maryland

CONTENTS

ABSTRACT

Meteor trail observations of the meridional mesospheric wind field are analyzed in terms of spherical harmonics which shows for the semiannual component a predominance in the P_3 term. This suggests two heat sources for the semiannual variations, one that peaks at the equator associated with the semiannual migration of the sun between the two hemispheres and a second heat input of greater magnitude that peaks at high latitudes. The latter is presumably related to auroral heating associated with the semiannual component in the occurrence of magnetic storms. The wind circulation, consistent with these sources, is shown to cause a semiannual redistribution of the minor constituent O in the lower thermosphere with the effects to decrease the ratios of O/N_2 and O/O_2 at high latitudes and to enhance these ratios at mid to low latitudes during equinox. This effect is consistent with the latitudinal structure in the semiannual component of the F_2 region ionization and mass spectrometer measurements of the O/O_2 ratio. As a consequence the pressure bulge in the O region of the thermosphere should be elongated around the equator and the semiannual variations in the exospheric temperature, deduced from satellite drag data at low inclination, should be too high. The model also reproduces the decrease in the relative concentration of O during summer consistent with the winter anomaly in the F_2 region.

SEMIANNUAL VARIATIONS IN THE NEUTRAL COMPOSITION

H. G. Mayr

H. Volland

INTRODUCTION

In an analysis of the semiannual effect in the F_2-region Mayr and Mahajan (1969) concluded that semiannual variations in the atmospheric composition (in particular the concentration of atomic oxygen) are required to understand the ionospheric behavior. This has been supported by the few measurements of $[O]/[O_2]$ which indicate a pronounced semiannual component as shown in Figure 1 (Table 1).

Johnson (1964) suggested meridional flow as a source for the semiannual temperature effect and Tohmatsu and Nagata (1963) considered global circulation as a possible explanation for the anomalous behavior in the latitudinal distribution of atomic oxygen (which was deduced from airglow observations).

In this paper we shall present a model in which global circulation, induced by solar radiation and auroral heating, is discussed as a mechanism to account for the semiannual effect in atomic oxygen.

WIND MODEL

Describing the wind field in terms of spherical harmonics, the equations of momentum and mass conservation are employed to determine the relations between meridional and vertical winds. As will be shown a posteriori the choice of spherical harmonics can be restricted such that we shall represent

in a first approximation the annual winds by

$$v_\theta^{(a)} \sim (v_{\theta 0} P_0 + v_{\theta 2} P_2) \sin\theta \cos\omega t$$

$$v_r^{(a)} \sim \frac{H}{r} (2 v_{\theta 1} P_1 + (-P_0 + 2P_3) v_{\theta 2}) \cos\omega t \qquad (1)$$

and the semiannual winds by

$$v_\theta^{(sa)} \sim (v_{\theta 1} P_1 + v_{\theta 3} P_3) \sin\theta \cos(2\omega t)$$

$$v_r^{(sa)} \sim \frac{H}{r} (2 v_{\theta 1} P_2 + 3.5 v_{\theta 3} P_4) \cos(2\omega t) \qquad (2)$$

with

$$\omega = \frac{2\pi}{1\ \text{year}}.$$

Here, (v_θ, v_r) are the latitudinal and the vertical wind components positive toward south and upward, respectively. $v_{\theta 0}, v_{\theta 1}, v_{\theta 2}, v_{\theta 3}$ are parameters to be determined from the wind measurements. H is an effective scale height determined by

$$\frac{1}{H} = \frac{1}{H_0} - \frac{1}{v_r} \frac{\partial v_r}{\partial r}$$

where H_0 is the density scale height.

There are several sources from which a qualitative picture of the global wind circulation can be deduced.

1) Meteor trail observations which provide information on atmospheric winds within the altitude range between 80 and 100 km.

2) Ionospheric observations which are suggestive of the global distribution of atomic oxygen thus producing information on the atmospheric circulation.

3) The pressure distribution in the upper atmosphere which in conjunction with the ionospheric behavior provides informations on the thermospheric wind field.

Mesospheric Winds

The mesospheric wind measurements deduced from meteor trail observations around 90 km (Kochanski, 1963) are shown in dashed lines in Figure 3. The winds are plotted versus season for Adelaide (35°S) and for Jodrell Bank (53°N).

With a Fourier analysis these wind velocities are separated into the annual and semiannual components at both stations to determine the latitude dependence at both frequencies in terms of spherical harmonics:

$$\text{annual} \ldots \quad v_{\theta 0} = 17 \text{ m/sec}, \quad v_{\theta 2} = -19 \text{ m/sec} \tag{3}$$

$$\text{semiannual} \ldots \quad v_{\theta 1} = 10 \text{ m/sec}, \quad v_{\theta 3} = 34 \text{ m/sec} \tag{4}$$

with these parameters the Equations (1) and (2) are defined:

$$v_\theta^{(a)} = (17\,P_0 - 19\,P_2)\sin\theta\cos\omega t \tag{5}$$

$$v_r^{(a)} = \frac{H}{r}(34\,P_1 - 19\,(-P_0 + 2P_3))\cos\omega t \tag{6}$$

$$v_\theta^{(sa)} = (10\,P_1 + 34\,P_3)\sin\theta\cos 2\omega t \tag{7}$$

$$v_r^{(sa)} = \frac{H}{r}(20\,P_2 + 120\,P_4)\cos 2\omega t \tag{8}$$

Equations 5 and 7 are combined to describe the seasonal variations (solid lines) at Adelaide and Jodrell Bank (Figures 2a and 2b respectively) which reflect a good representation of the wind measurements.

Based on this analysis a schematic picture of the thermospheric circulation can be drawn (Figure 3).

Applying a well known circulation theorem of meteorology we expect the winds to rise above the region of the maximum heat input and to descend above the region of the minimum heat input. Accordingly, we can infer a gross picture of the energy distribution from Figure 3, suggesting maxima in the energy input at the locations indicated by Q.

Ionospheric Effects

The ionosonde data discussed in Mayr and Mahajan (1969) have been chosen for 1600 LT and from northern latitudes in the American longitude zone. We

supplemented these data with those from South American latitudes. Performing a Fourier analysis for both maximum (1958, 1959) and minimum (1963, 1964) solar activity conditions the relative amplitudes $\Delta N_m / N_m$ of the semiannual effect were deduced.

The results are shown in Figure 4 and it is apparent that the effects are very similar for both activity conditions (the dashed line is a mean square fit through all the data points). They show pronounced masima between 30° and 40° latitudes with relative amplitudes as high as 40%.

Concurring with Mayr and Mahajan (1969) that the semiannual effect in the ionosphere is primarily induced by semiannual variations in the neutral composition we suggest then that the semiannual effect in the $[O]/[N_2]$ and $[O]/[O_2]$ ratios peaks at 30° to 40° latitudes. It will be shown later that this feature supports the circulation field discussed in the previous figure.

Thermospheric Effects

A development of exospheric temperature data that were derived from satellite drag measurements (Jacchia and Slowey, 1964; Jacchia et al., 1966) into a series of spherical harmonics

$$T \sim \cdots - T_1 P_1 \cos \omega t + T_2 P_2 \cos 2\omega t$$

gives the annual and semiannual components

$$T_1 \sim T_2 \sim 50° K$$

at medium solar activity. The direction of the temperature field and thus the pressure gradient is from the summer to the winter hemisphere for the annual component and from the equator toward higher latitudes for the semiannual component. At F2 layer heights the relative pressure variation equivalent to the exospheric temperature variation of 50°K is according to the Jacchia model

$$\left|\frac{P_{10}}{P_{00}}\right| \sim \left|\frac{P_{20}}{P_{00}}\right| \sim 0.33$$

at 250 km altitude. We can estimate the magnitude of the horizontal winds due to these pressure gradients from the equation of conservation of momentum. Assuming the collision frequency ν to be much larger than the angular velocity Ω of the earth's rotation one obtains

$$v_0^{(a)} \sim -v_1^{(sa)} \sim \frac{c^2}{\nu\gamma r}\frac{P_1}{P_0} \sim 50 \text{ m/sec} \qquad (9)$$

where $v_0^{(a)}$ and $v_1^{(sa)}$ are the coefficients of the latitudinal winds in Equations 1 and 2. c ~800 m/sec is the velocity of sound, $\gamma = 1.5$ is the ratio of the specific heats and $\nu \sim 6\,\Omega$ is the ion collision frequency. Further support of the existence of such a wind field within the thermsophere comes from an analysis of the seasonal behavior of the F2 region as demonstrated by Brinton et al. (1969) and by Mayr and Mahajan (1969). Moreover, the latitudinal dependence of the thermospheric helium distribution allows to deduce informations on the global circulation (Reber et al., 1970) which also suggests meridional winds from the summer to the winter hemisphere during solstice conditions.

ENERGETICS

The solar heat input per unit area can be considered in a first order approximation to be proportional to $\cos\chi$, where χ is the zenith distance. Averaged over a day the total amount of solar heat input per unit area is then

$$q \propto \int_{-\tau_0}^{\tau_c} \cos\chi \, d\tau = 2\left\{\sin\theta\cos\gamma\cos\tau_c + \tau_0 \sin\theta\sin\gamma\right\} \qquad (10)$$

with

$$\tau_0 = -\arccos\left\{\frac{\tan\gamma}{\tan\theta}\right\}$$

$$\delta = \delta\cos\omega t$$

θ co-latitude

δ maximum solar declination

$$\omega = \frac{2\pi}{1\ \text{year}} = 2\times 10^{-7}\ \text{sec}^{-1}\ \text{angular frequency of one year}.$$

t is the universal time with t = 0 at the beginning of the year.

For solstice and equinox conditions relation (10) is shown in Figure 5. From a Fourier analysis we determine the annual and semiannual components of q. These Fourier components of q are developed in the form

$$q^{(a)} \sim -q_1 P_1 \cos\omega t$$

$$q^{(sa)} \sim q_2 P_2 \cos 2\omega t \qquad (11)$$

where P_n are the Legendre polynoms.

The dashed lines in Figure 5 give the functions

$$1.25\,P_1 \text{ (annual)}$$
$$-\,0.4\,P_2 \text{ (semiannual)} \qquad (12)$$

which represent the Fourier components of q (Equation 10) closely.

We notice two characteristics in Figure 5 which are of particular interest. The input has a maximum at high latitudes and not at the subsolar point during the solstices, and the semiannual component is rather strong, almost one third of the annual component.

Considering the energy and momentum equations one can verify (see e.g. Volland and Mayr, 1968) that the latitude and time dependence of the pressure and vertical wind fields follow very closely the distribution of the energy input,

$$v_r \propto p \propto q$$

Thus, we can compare the annual and semiannual components of the solar heat input (Equation 12) with the vertical wind field components deduced from meteor trail observations in the mesosphere (Equations 6 and 8) and with the pressure field deduced from drag measurements in the thermosphere (Equation 9). In Table 2 these parameters are summarized.

Table 2

The Relative Magnitudes of the Annual and Semiannual Components

	Heat Input (solar radiation)	Vertical Winds Mesosphere	Pressure Thermosphere
Annual	P_1	$P_1 - 0.5(-P_0 + 2P_3)$	P_1
Semiannual	$- 0.3 P_2$	$0.7P_2 + 3.5P_4$	$-P_2$

Table 2 indicates that:

1) The magnitude of the semiannual component in the solar input which peaks at the equator is by almost a factor of three too low to account for the semiannual component in the thermospheric pressure field.

2) The strong P_4 term in the semiannual component of the mesospheric circulation suggests two heat sources. One that peaks at the equator presumably due to solar radiation and one that peaks at high latitudes presumably associated with the semiannual component in the occurrence of magnetic storms.

3) The P_2 term in the semiannual component of the thermosphere stems from satellite drag data that were derived from a height region where atomic oxygen is the predominant constituent. Considering that O is affected by the dynamics in the N_2 region it is then understandable that its latitudinal structure is different from that at lower altitudes where P_4 is dominant.

NEUTRAL COMPOSITION

Below 90 km photochemical reactions determine the concentration of atomic

oxygen while above that height transport processes become increasingly important. This is true in particular for transport processes induced by atmospheric winds whose magnitudes tend to increase with height.

Colegrove et al., (1965) performed an extensive theoretical study on the distribution of atomic and molecular oxygen in the lower atmosphere (70-140 km) discussing photodissociation, recombination and diffusion as the dominating processes (we shall refer to their paper by (C)). Taking the oxygen absorption spectrum from measurements of Watanabe et al., (1963) and Metzer and Cook (1964), and the solar emission spectrum from Detwiler et al., (1961), (C) calculated the photodissociation rates as a function of the O_2 column density. Thereby they assumed an average slant path angle of 45° thus approximated an average number of dissociations per day. Dividing their column densities by the O_2 scale height, we derived the rate coefficient for O_2 dissociation, q as a function of the O_2 concentration (Figure 6).

Atomic oxygen is removed by the three body recombination processes

$$O + O + M = O_2 + M, \tag{13}$$

for which in the case of M N the rate coefficient is

$$\alpha_1 = 3.0 \times 10^{-33} (T/300)^{-2.9}$$

(Campbell and Thrush, NASA Reaction Rate Handbook, 1967), and

$$O + O_2 + M \rightarrow O_3 + M \qquad (14)$$

with a reaction rate coefficient of

$$\alpha_2 = 5.5 \times 10^{-34} (T/300)^{-2.6}$$

(Kaufman and Kelso, 1964).

Below 100 km eddy diffusion is the predominant diffusion mechanism. By matching their theoretical results with $[O]/[O_2]$ measurements, (C) derived the eddy diffusion coefficient K to be

$$K = 4 \times 10^6 \text{ cm}^2 \text{ sec}^{-1} .$$

Above 120 km molecular diffusion prevails. For the diffusion of O through O_2 and N_2 we adopt

$$D = 0.26 \left(T/T_0\right)^{1.75} \left(p/p_0\right)^{-1} ,$$

an experimental result arrived at by Walker (1961). T_0 and p_0 are standard temperature and pressure. p is the sum of the partial pressures of N_2 and O_2.

Estimating the characteristic times of the various processes described above one finds at 100 km

$$t_{dissociation} = [O]/q\,[O_2] \sim 10 \text{ days}$$

$$t_{recombination} = \left([N_2]\,[O]\,\alpha_1\right)^{-1} \sim 1000 \text{ days}$$

$$t_{eddy\ diffusion} = H^2/K \sim 10 \text{ days}$$

hence, as already (C) concluded, diurnal variations cannot be excited in the composition of the lower atmosphere. The period of half a year, however, is long when compared with the shortest characteristic times referred to above and therefore one can expect semiannual or annual variations in the atmospheric composition.

With these processes the continuity equation for O has the form

$$2q[O_2] - [O]\,[N_2]\left(2\alpha_1\,[O] + \alpha_2\,[O_2]\right)$$

$$- \frac{\partial}{\partial r}\left([O]\,v_{or}\right) - \frac{1}{r \sin\theta}\frac{\partial}{\partial \theta}\left([O] \sin\theta v_{o\theta}\right) = 0 \qquad (15)$$

where v_{or} and v_o are the transport velocities of O in the radial and latitudinal directions. Due to the fact that the period of half a year is large when compared with the characteristic times of the dominant processes it is justified to consider oxygen in quasi steady state ($\partial/\partial t = 0$).

The equation of momentum conservation in the r direction is

$$[O]\,(v_{or} - v_r) = -D\left(\frac{\partial [O]}{\partial r} + \frac{[O]}{T}\frac{\partial T}{\partial r} + \frac{mg}{kT}[O]\right)$$

$$- K\left(\frac{\partial [O]}{\partial r} + \frac{[O]}{T}\frac{\partial T}{\partial r} + \frac{\bar{m}g}{kT}[O]\right); \qquad (16)$$

v_r is the radial (vertical) wind velocity, m_0 the mass of O, $\bar{m}$ the average molecular mass and k is the Boltzmann constant.

In the meridional direction the drag term ($[O]\,(v_{o\theta} - v_\theta)$) dominates the lateral momentum transfer thus we can assume

$$v_{o\theta} = v_\theta , \qquad (17)$$

v_θ being the meridional wind component. Furthermore we neglect the meridional variations in the particle concentrations as we consider them as small compared with the latitudinal variations of the wind velocity. Consequently the continuity Equation (16) becomes

$$2q[O_2] - [O]\,[N_2]\,(2\alpha_1\,[O] + \alpha_2\,[O_2]) - \frac{\partial}{\partial r}\left([O]\,(v_{or} - v_r)\right)$$

$$= \frac{\partial}{\partial r}\left([O]\,v_r\right) + \frac{[O]}{r\sin}\frac{\partial}{\partial \theta}\left(\sin\theta v_\theta\right) . \qquad (18)$$

The lateral and vertical wind velocities that occur in Equation (18) are related through the continuity equation

$$\frac{\partial N}{\partial t} = -\frac{\partial (N v_r)}{\partial r} - \frac{1}{r \sin\theta} \frac{\partial}{\partial \theta} \left(N \sin\theta v_\theta \right) = 0 , \qquad (19)$$

where N is the total mass density ($N = m_o [O] + m_{N_2} [N_2] + m_{o_2} [O_2] + \cdots$). Our estimations which are based on wind measurements and on the semiannual density amplitudes derived by Volland (1969), indicates that the temporal density variations are negligible ($\partial/\partial t = 0$). Again neglecting the latitudinal variations in the total density, the relation

$$\frac{1}{r \sin\theta} \frac{\partial}{\partial \theta} \left(\sin\theta v_\theta \right) = \frac{v_r}{H} - \frac{\partial v_r}{\partial r} \qquad (19a)$$

evolves, H being the density scale height. With (19), Equation (18) finally takes the form

$$2q[O_2] - [O] [N_2] \left(2\alpha_1 [O] + \alpha_2 [O_2] \right) - \frac{\partial}{\partial r} \left([O] \left(v_{or} - v_r \right) \right)$$

$$= v_r \frac{\partial}{\partial r} [O] + \frac{v_r}{H} [O] . \qquad (20)$$

The right hand side of (20) describes the wind effect. For an upward directed (positive) wind velocity both expressions are positive definite below the height where atomic oxygen has its maximum concentration (about 100 km). Above

that height the scale height of O is nearly twice that of H in the region where N_2 is the major constituent and it becomes equal to H at heights where O is the major species; the sum of both expressions thus has always the same sign as the vertical velocity. For this reason an upward wind acts like a particle sink and hence decreases atomic oxygen, while a downward wind constitutes a particle source that enhances the oxygen concentration.

We define with r_∞ the height at which the constituent O becomes predominant; then it follows

$$v_{or} = v_r \quad \text{at} \quad r = r_\infty$$

and the integration of (20) yields

$$[O]\ (v_{or} - v_r) = \int_r^{r_\infty} \left(2q\ [O_2] - [O]\ [N_2]\ (2\alpha_1\ [O] + \alpha_2\ [O_2])\right) dr$$

$$- \int_r^{r_\infty} \left(v_r \frac{\partial [O]}{\partial r} + \frac{v_r}{H}\ [O]\right) dr \,. \qquad (21)$$

The diffusion velocity $(v_{or} - v_r)$ affects the oxygen distribution (Equation (20)) primarily at lower altitudes where the atmospheric density is high. The magnitude of the diffusion velocity, however, depends on the wind interaction over the entire altitude range in which the constituent under consideration is a minor species (see second part on the right hand side of Equation (21)). Since this is true for

any minor constituent, the wind effects on oxygen and helium f.e. can be significantly different due to the fact that the wind interaction reaches only up to 200 km for oxygen, but up to at least 600 km for helium, the heights at which these species become prevailing. In a nondissipative medium the wind velocities tend to increase with a scale height close to that of the major constituents. For this reason it is essentially the wind interaction at high altitudes that contributes to the diffusion flux. In the following section we shall therefore primarily discuss the implications of the thermospheric wind circulation.

Equation (20) and (21) are two coupled non-linear differential-integral equations which describe the distribution of atomic oxygen, similar equations can be derived for O_2. The solution for [O] is uniquely determined if one considers that this species approaches photochemical equilibrium at lower altitudes. For O_2 we chose as boundary condition the value

$$[O_2]_{70\ km} = 1.3 \times 10^{14}/cc$$

which is consistent with atmospheric models, and we assume its vertical transport velocity to be equal to the wind velocity at the upper boundary of our calculations (at 200 km).

DISCUSSION

Qualitative

There are some obvious implications of the thermospheric wind circulation that was schematically described in Figure 3. During solstice the vertical winds are upward in the summer hemisphere and downward in the winter hemisphere. The effect is to decrease the atomic oxygen concentration in summer and to increase it in winter. This process was suggested by Kellogg (1961) to explain the winter anomaly in the F_2 -region.

During equinox the wind velocities are directed downward at midlatitudes (40°) and upward at the equator and at high latitudes. As a consequence, the atomic oxygen concentration should be enhanced at midlatitudes. This feature is entirely consistent with observations of the $[O]/[O_2]$ ratio that was sampled predominantly at these midlatitudes. Furthermore the observations of the seasonal variations in the ionosphere reveal peaks in the F_2 -region at midlatitudes and during equinox as is apparent from the semiannual component shown in Figure 4. This ionospheric effect reflects upon enhancements in the oxygen concentration as shown in Mayr and Mahajan (1969). The magnitude of the ionospheric effect is somewhat too small to correlate quantitatively with the observations of atomic oxygen. This discrepancy, however, can be easily explained if one considers that at ionospheric heights (that is in the upper part of the thermospheric circulation cell (Figure 3)) the wind component along the magnetic field applies a downward drag force on the ions and this decreases the electron density concentration at the height of the F_2 -peak.

Quantitative

To compute the wind effects on atomic oxygen we adopted the latitudinal variation in the vertical wind field as described in Equations 6 and 7.

$$v_r(\theta, r) = \left(v_{r1} P_1 + v_{r3}\left(-P_0 + 2P_3\right)\right) \cos(\omega t - \rho) + \left(v_{r2} P_2 + v_{r4} P_4\right) \cos(2\omega t - 2\rho), \quad (22)$$

where ρ is a phase parameter that was chosen to optimally fit the measurements ($\rho = 30°$). At 90 km the wind parameters are related to the mesospheric wind measurements. Assuming a scale height of

$$H = 4 \text{ km}$$

the vertical wind velocity can be deduced

$$v_{r1} = \frac{Hu_{\theta 0}}{r} = 2.1 \text{ (cm)}$$

$$v_{r3} = \frac{Hu_{\theta 2}}{r} = -1.2 \text{ (cm)}$$

$$v_{r2} = \frac{Hu_{\theta 1}}{r} = 1.3 \text{ (cm)}$$

$$v_{r4} = \frac{Hu_{\theta 3}}{r} = 7.5 \text{ (cm)}.$$

We assumed that the scale height H of the vertical velocity varies between 4 km at mesospheric heights up to infinite in the thermosphere at 250 km where due to viscosity and ion drag the wind velocities become height independent. The magnitude of the wind velocity was thereby assumed to vary by a factor of 10 between 90 and 200 km.

In Figure 7 the computed distribution of O and O_2 is shown for wind velocities between -60 and +60 cm/sec at 200 km (and corresponding variations of -6 to +6 cm/sec at 100 km). Figure 5 presents the wind induced variability of atomic oxygen at 120 km in the form of the relative amplitude

$$C = \frac{\Delta [0]}{[0]} = \frac{[0](-v) - [0](+v)}{2[0](0)}$$

which is plotted as a function of (v). This relation reflects an almost linear velocity dependence and accordingly implies that the relative magnitudes of composition effects can be directly inferred from the relative magnitudes of the wind field.

Also shown in Figure 7 is the relative amplitude of the $[O]/[O_2]$ ratio

$$D = \frac{\Delta \frac{[0]}{[O_2]}}{\frac{[0]}{[O_2]}} = \frac{\frac{[0]}{[O_2]}(-v) - \frac{[0]}{[O_2]}(+v)}{2\frac{[0]}{[O_2]}(0)}$$

which is slightly more sensitive to the wind effects.

Employing Equation 22 we computed the $[O]/[O_2]$ ratio for 35° latitude which corresponds to the latitude range (33° to 40°) the $[O]/[O_2]$ data were

primarily sampled from. The theoretical results are shown as solid lines which reveal an excellent agreement with the observations. The theoretical variations in the $[O]/[O_2]$ ratio reveal in particular a) enhancements during equinox periods which are consistent with the semiannual variations in the F_2 region and b) a winter to summer decrease by about a factor of two which is consistent with the variations required to explain the winter anomaly in the F_2 region.

CONCLUSION

The composition measurements of the $[O]/[O_2]$ ratio at 120 km which were shown to exhibit a significant semiannual component (Mayr and Mahajan 1969) have been interpreted in terms of global circulation. The circulation pattern consistent with these observations has been inferred from mesospheric wind measurements and from the latitudinal structure in the semiannual effect of the F_2 -region.

Based on the overall consistency of these phenomena we conclude that the semiannual effect in the dynamics of the upper atmosphere is induced by:

a) the solar radiative heat input which has a semiannual component that peaks at the equator and

b) an even stronger peak in the heat input at high latitudes (auroral zone) which is presumably associated with the semiannual component in the occurrence of magnetic storms (Priester and Cattaui (1961).

The circulation induced by these sources produces an upwelling of air with a depletion of atomic oxygen at high latitudes and a subsiding of air with an

enhancement of atomic oxygen at mid to low latitudes. The implications are that the pressure bulge in the O region should be elongated around the equator which would be consistent with observations by Jacchia and Slowey (1966). Furthermore, the semiannual variations in the neutral composition discussed in this paper support that the semiannual effect in the exospheric temperature is smaller at moderate latitudes than indicated from the analysis of satellite drag data in which variations of the composition at the turbo pause have been entirely neglected.

ACKNOWLEDGMENT

We are indebted to G. P. Newton for valuable and stimulating discussions.

REFERENCES

1. Brinton, H. C., H. G. Mayr, R. A. Pickett and H. A. Taylor, Jr., The Effect of Atmospheric Winds on the O^+-H^+ Transition Level, Space Research X, 1970.

2. Campbell, I. M., and B. A. Toush, in DASA Reaction Rate Handbook, 1962.

3. Colegrove, F. D., W. B. Hanson, and F. J. Johnson; Eddy Diffusion and Oxygen Transport in the Lower Thermosphere, J. Geophys. Res., 70, 4931-4941, 1965.

4. Detwiler, C. R., D. L. Lamelt, J. D. Purcell and R. Tousey, The Intensity Distribution in the Ultraviolet Solar Spectrum, Symposium D'Aeronomy, 9-18, Paris, 1961.

5. Elford, W. G., A Study of Winds Between 80 and 100 km, Planetary Space Sci., 1, 94-101, 1959.

6. Greenhow, J. S., and E. L. Neufeld, Large Scale Irregularities in High Altitude Winds, Proc. Phys. Soc. London, 75, 228-234, 1960.

7. Gross, J., D. Offermann, and U. von Zahn, Neutral Particle Densities in the Lower Thermosphere as Measured by Mass Spectrometers Above Fort Churchill and Sardinia, Space Res., 8, 920-925, 1968.

8. Hedin A. E., and A. O. Nier, A Determination of the Neutral Composition, Number Density, and Temperature of the Upper Atmosphere from 120 to 200 Kilometers with Rocket Borne Mass Spectrometers, J. Geophys. Res., 71, 4121-4131, 1966.

9. Jacchia, L. G., Static Diffusion Models of the Upper Atmosphere with Empirical Temperature Profiles, Smithsonian Institution, Astrophysical Observatory, Special Report No. 170, Cambridge, Mass., 1964.

10. Jacchia, L. G. and J. Slowey, The Shape and Location of the Diurnal Bulge in the Upper Atmosphere, Space Res. VII, p. 1077-1090, North-Holland Publishing Company, Amsterdam, 1967.

11. Johnson, F. S., Circulation at Ionospheric Levels, Report of the Southern Center of Advanced Studies, Contract CW-II, 10531, 1964.

12. Kasprzak, W. T., D. Krankowsky, and A. O. Nier, A Study of Day-Night Variations in the Neutral Composition of the Lower Thermosphere, J. Geophys. Res., 73, 6765-6782, 1968.

13. Kaufman, F., and J. R. Keho, Rate Constant of the Reaction $O + 2O_2 \rightarrow O_3 + O_2$, J. Chem. Phys., 40, No. 4, 1964.

14. Kellogg, W. W., Chemical Heating Above the Polar Mesosphere in Winter, J. Meteorology, 18, 373-381, 1961.

15. Kochanski, A., Circulation and Temperatures at 70- to 100-Kilometer Height, J. Geophys. Res., 68, 213-226, 1963.

16. Krankowsky, D., W. T. Kasprzak, and A. O. Nier, Mass Spectrometer Studies of the Composition of the Lower Thermosphere During Summer 1967, J. Geophys. Res., 73, 7291-7306, 1968.

17. Mauersberger, K., D. Müller, D. Offermann, and U. von Zahn, Neutral Constituents of the Upper Atmosphere in the Altitude Range of 110 to 160 km Above Sardinia, Space Res., 7, 1150-1158, 1967.

18. Mayr, M. G., and K. Mahajan, Seasonal Variations in the F_2 Region, NASA Document X-621-69-255, 1969, in press for J. Geophys. Res.

19. Metzger, P. M., and G. R. Cook, A Reinvestigation of the Absorption Cross Sections of Molecular Oxygen in the 1050-1800 A Region, J. Quantitative Spectroscopy Radiative Transfer, 4, 107-116, 1964.

20. Nier, A. O., J. H. Hoffman, C. Y. Johnson, and J. C. Holmes, Neutral Composition of the Atmosphere in the 100- to 200-Kilometer Range, J. Geophys. Res., 69, 979-989, 1964.

21. Pokhunkov, A. A., On the Variation in the Mean Molecular Weight of Air in the Night Atmosphere at Altitudes of 100 to 210 km from Mass Spectrometer Measurements, Planetary Space Sci., 11, 297-304, 1963a.

22. Pokhunkov, A. A., Gravitational Separation, Composition and Structural Parameters of the Night Atmosphere at Altitudes Between 100 and 210 km, Planetary Space Sci., 11, 441-449, 1963b.

23. Pokhunkov, A. A., Gravitational Separation Composition, and the Structural Parameters of the Atmosphere at Altitudes Above 100 km, Space Res., 3, 132-142, 1963c.

24. C. A. Reber, H. G. Mayr and P. Hays, Thermospheric Wind Effects on the Global Distribution of Helium, EOS, 1970.

25. Schaefer, E. J., and M. H. Nichols, Upper Air Neutral Composition Measurements by a Mass Spectrometer, J. Geophys. Res., 69, 4649-4660, 1964.

26. Schaefer, E. J., Neutral Composition, Sci. Rept. 05627-3-S, High Altitude Eng. Lab., The University of Michigan, 1966.

27. Schaefer, E. J., Temperature and Composition of the Lower Thermosphere Obtained from Mass Spectrometer Measurements, Space Res., 8, 959-968, 1967.

28. Tohmatsu, T., and T. Nagata, Dynamical Studies of the Oxygen Process Line in the Airglow, Planet. Space Sci., 10, 103-116, 1963.

29. Volland, H., A Theory of Thermospheric Dynamics. Part II: Geomagnetic Activity Effect, 27 Day Variation and Semiannual Variation, Planet. Space Sci., 1969.

30. Walker, R. E., Measurement of the O-O Diffusion Coefficient, J. Chem. Phys., 31, 2196-2197, 1961.

31. Watanabe, K. E., C. Y. Inn, and M. Zelikoff, Absorption Coefficients of Oxygen in the Vacuum Ultraviolet, J. Chem. Phys., 21, 1026-1030, 1953.

Table 1

O and O_2 Number Density Ratios at 120 km Measured by

Rocket-Borne Mass Spectrometers

(from Mayr and Mahajan, 1969)

Date	$S_{10.7}$	Time	Latitude	$n(O)/n(O_2)$	Reference
Sept. 23, 1960	175	0050 LT	'Middle'	0.72	Pokhunkov (1963a, b, c)
May 18, 1962	95	1302 EST	38°N	(1.2)	Schaefer and Nicholas (1964)
Mar. 28, 1963	73	0255 LT	38°N	1.2	Schaefer (1966)
June 6, 1963	77	0730 MST	33°N	1.1	Hedin et. al. (1964)
Nov. 26, 1963	82	1316 LT	38°N	1.2	Schaefer (1967)
Feb. 18, 1965	72	1409 LT	59°N	0.75	Schaefer (1967)
Feb. 19, 1965	72	0317 LT	59°N	0.75	Schaefer (1967)
Apr. 15, 1965	75	0345 MST	33°N	0.33	Hedin and Nier (1966)
Nov. 30, 1966	75	0445 MST	33°N	(0.5)	Kasprzak et. al. (1968)
Dec. 2, 1966	98	1409 MST	33°N	0.46	Kasprzak et. al. (1968)
Dec. 11, 1965	76	0505 MET	40°N	1.56	Mauersberg et. al. (1967)
Dec. 12, 1966	163	1320 CST	59°N	0.87	Gross et. al. (1968)
June 21, 1967	119	1249 MST	33°N	0.55	Krankowsky et. al. (1968)
July 20, 1967	131	0200 MST	33°N	0.41	Krankowsky et. al. (1968)
July 20, 1967	131	1224 EST	33°N	0.41	Krankowsky et. al. (1968)

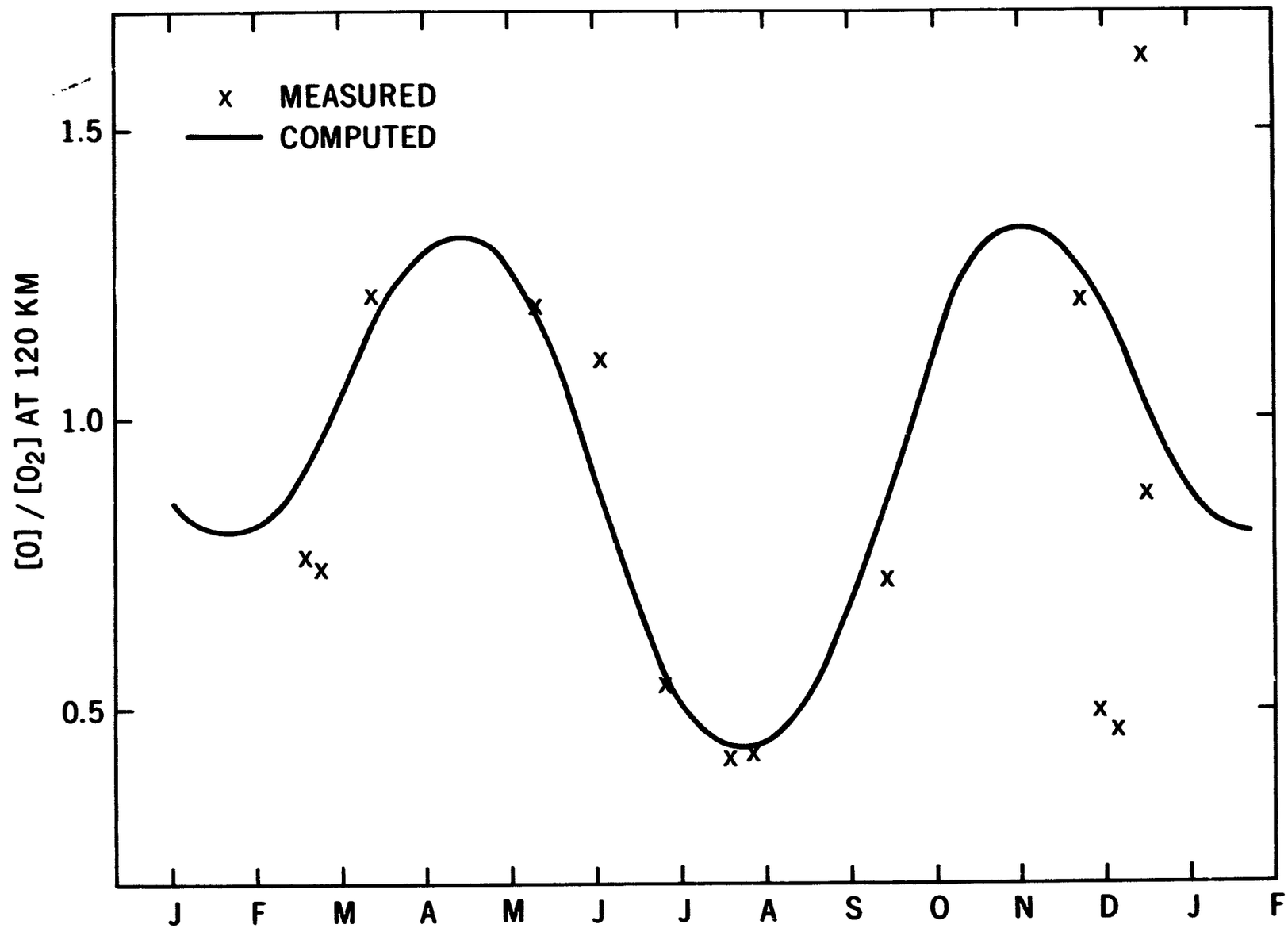

Figure 1. Stars show the $[O]/[O_2]$ measurements from 120 km which exhibit a semiannual effect (Mayr and Mahajan 1969). The solid line represents the calculated variations due to global circulation.

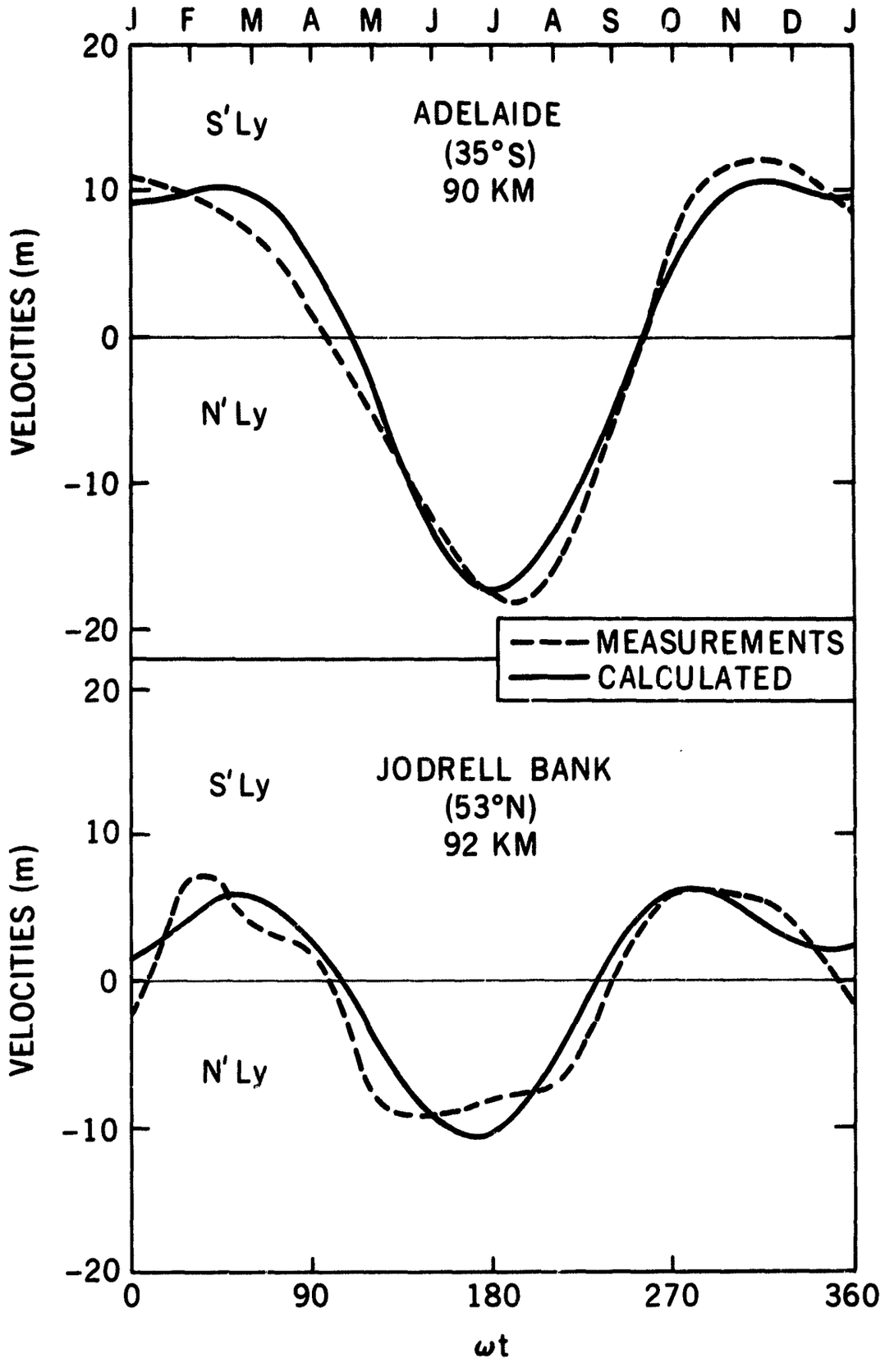

Figure 2. Mesospheric wind measurements from Adelaide (35°S) and Jodrell Bank (53°N) as shown in Kochanski (1963). Solid lines show the wind magnitudes calculated from the wind model.

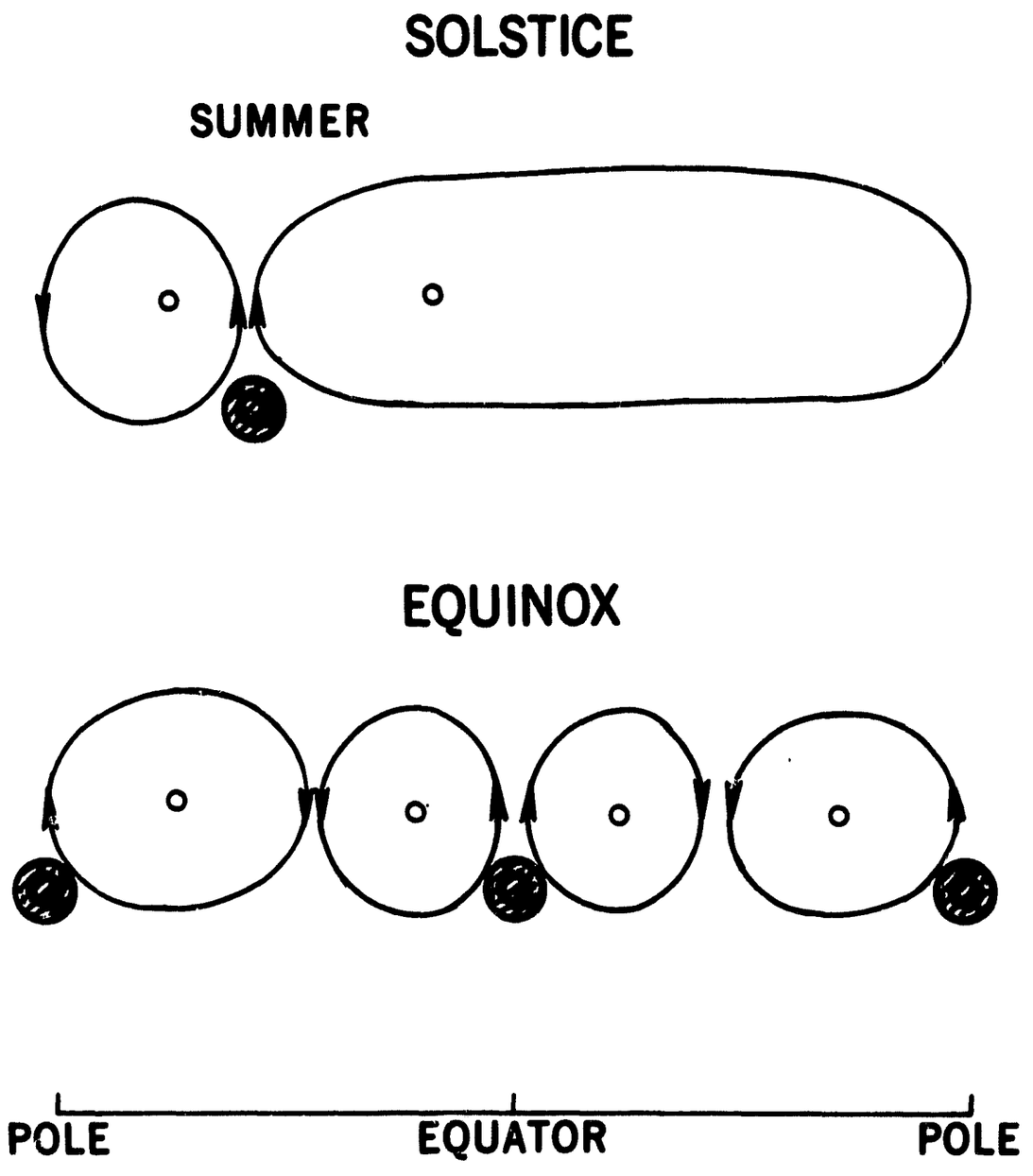

Figure 3. Schematic circulation for solstice and equinox inferred from mesospheric wind measurements.

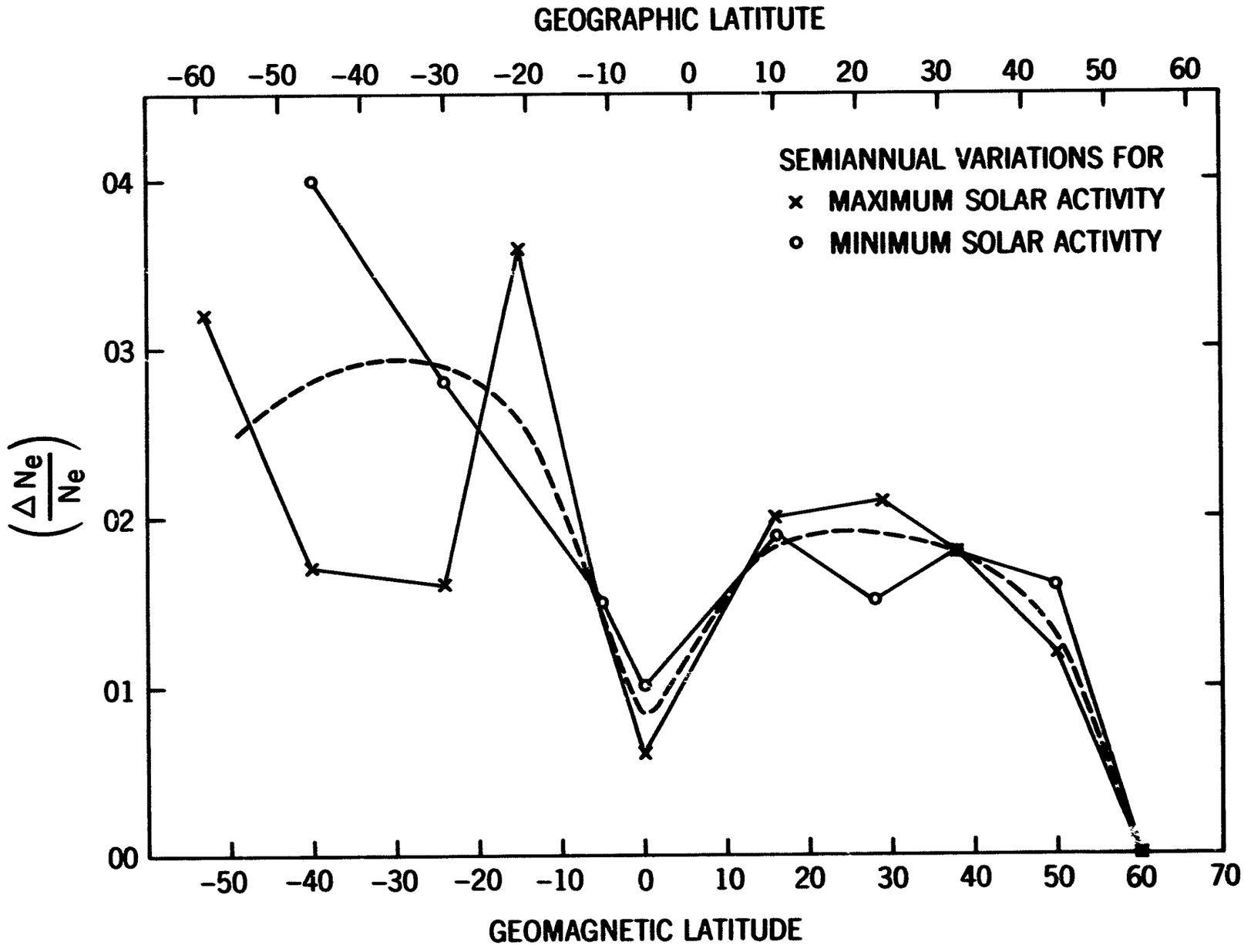

Figure 4. The relative amplitude of the semiannual effect at the height of the F_2 peak deduced from ionosonde measurements at 1600 LT at American longitudes for 1958-1959 (maximum solar activity) and 1964-1965 (minimum solar activity). The dashed line represents the average effect which seems almost independent of the solar activity.

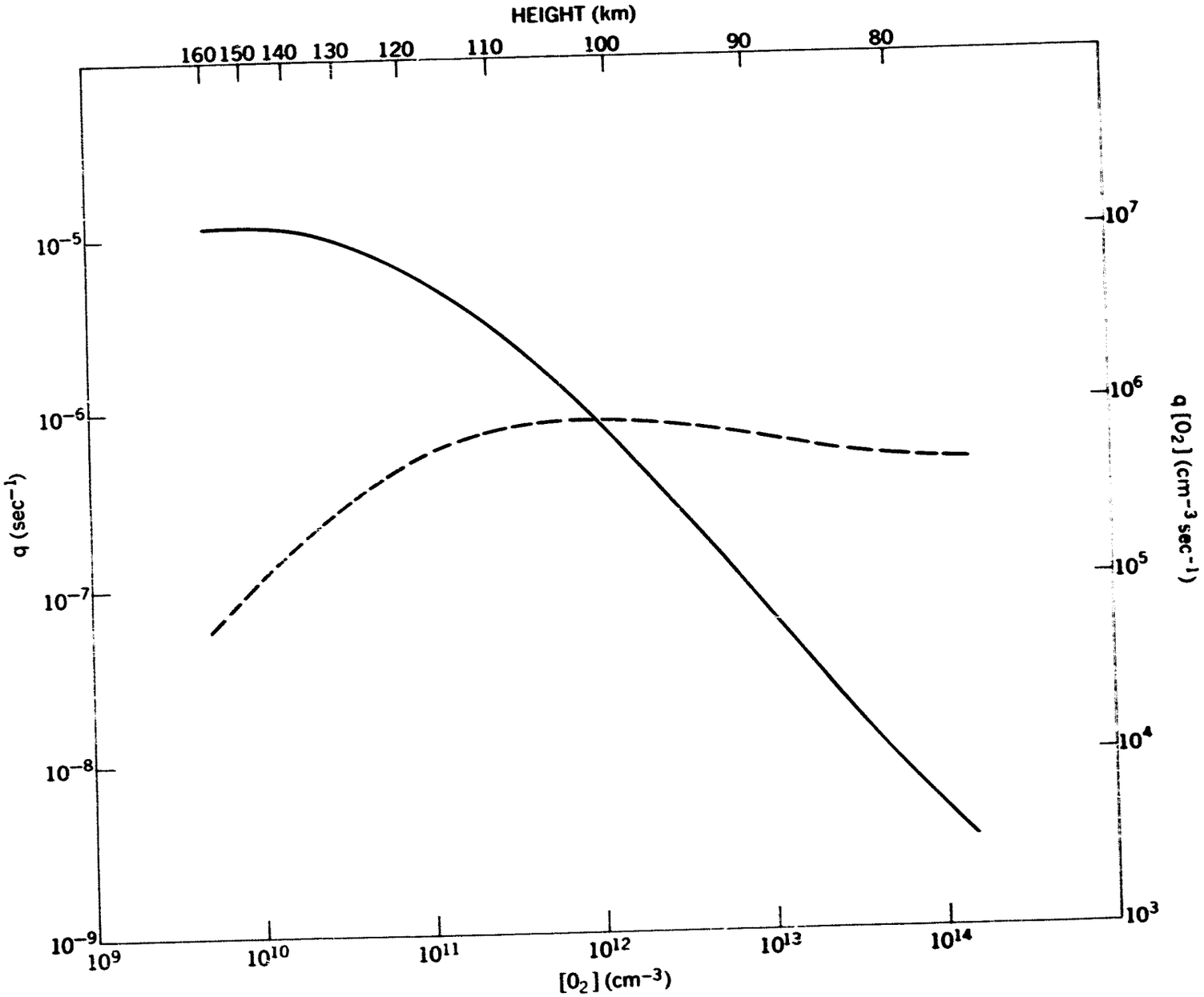

Figure 6. Dissociation-rates (dashed line) and rate coefficients plotted versus height

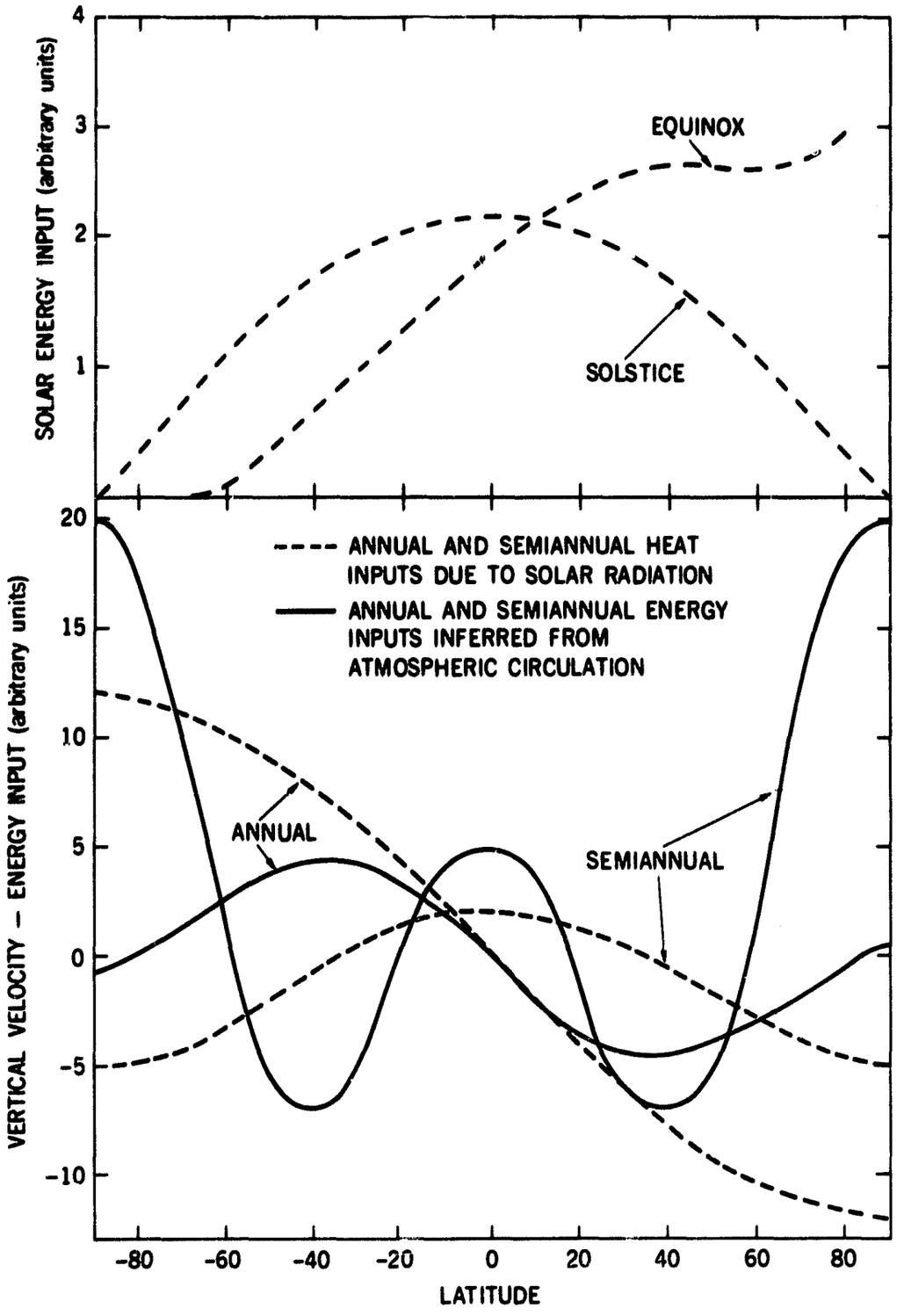

Figure 5. The solar heat input per unit area is shown in arbitrary units in Figure 5a (note the peak at high latitudes during solstice). The annual and semiannual components of the solar input are shown as dashed lines in Figure 5. The solid lines in Figure 5b represent the annual and semiannual energy distributions as deducted from the mesospheric wind measurements.

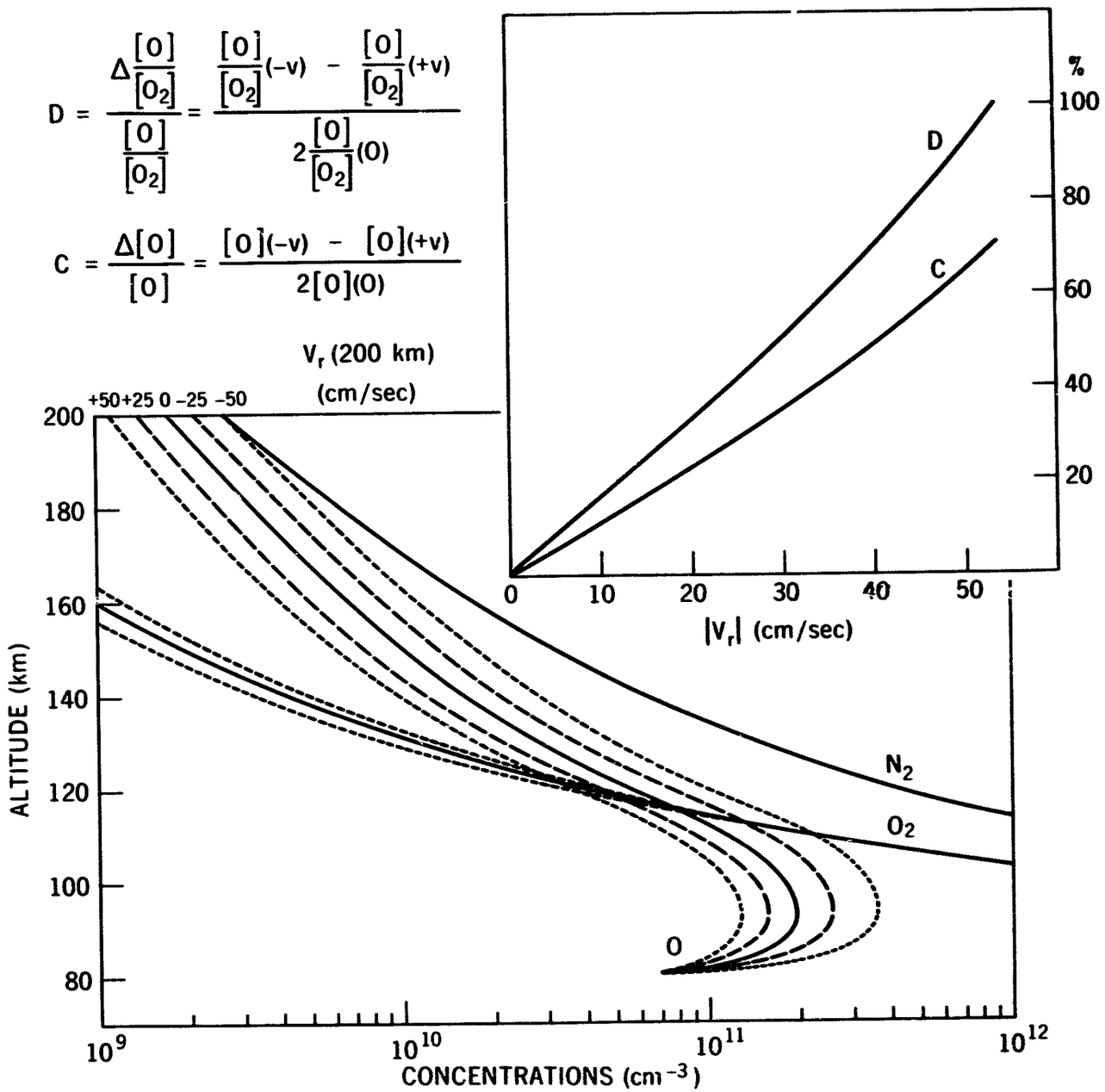

Figure 7. Height distributions of O and O_2 computed for various wind velocities. The relative amplitudes of variations in [O] and $[O]/[O_2]$ at 120 km are shown; note the linear dependence on the wind magnitude.